Analytical solutions of strain energy density for steel load-carrying cruciform welded joints under tension and bending loading

Wei Song[1,2], Xuesong Liu[1,*], S.M.J. Razavi[2]

1. State Key Laboratory of Advanced Welding and Joining, Harbin Institute of Technology, Harbin 150001, China.
2. Department of Mechanical and Industrial Engineering, Norwegian University of Science and Technology (NTNU), Richard Birkelands vei 2b, 7491 Trondheim, Norway.

Abstract

In this paper, we develop an analytical model to calculate the notch Strain Energy Density (SED) of Load-carrying Cruciform Welded Joints (LCWJ) for fatigue assessment. The analytical solutions are applied to explain the geometry effects of LCWJ under cyclic tension and bending comprehensively, such as the weld size, plate thickness, and weld penetration. For the sake of these solutions, it further determines SED values rapidly without any Finite Element (FE) calculation. The Notch Stress Intensity Factor (NSIF) and SED values obtained according to the proposed analytical solution are firstly validated by comparing finite element data from several stimulations in terms of LCWJ models, resulting in a good agreement. Moreover, the failure transition relationship between weld toe and weld root is assured by the analytical equation. The transition evolution under different notch angles according to SED results is investigated. As a preliminary validation, the accuracy and reliability of proposed analytical model in this paper are checked by several experimental data generated from testing under fatigue loading. The good agreements between the experimental results and existing scatter bonds based on SED, NSIF and peak stress fatigue design standards establish reliable basis for validation of the present analytical equations. Therefore, these analytical equations provide an alternative to FEM for engineering applications.

* Corresponding author. Tel.: +86 451 86418433; fax: +86 451 86416186.

E-mail address:

liuxuesong@hit.edu.cn (Xuesong Liu)

Nomenclature:

a, crack length; α, notch opening angle; e_i, parameters dependent on the opening angle; $\Delta\sigma_n$, remotely applied stress; E, Young's modulus; ETS, Effective Traction Stress; EETS, Equivalent Effective Traction Stress; FE, Finite Element; FEA, Finite Element Analysis; h, weld size; k_i, non-dimensional coefficients; K_i^*, non-dimensional parameters; ΔK_i stress intensity factors; L, attachment plate thickness; LCWJ, Load-carrying Cruciform Welded Joints; NSIF, Notch Stress Intensity Factor; p, lack of penetration; q, geometry parameter; R_c, radius of the semicircular sector; SED, Strain Energy Density; θ, weld toe flank angle; t, the plate thickness; v, Poisson's ratio; W_i, weld number;

Keywords

Analytical solutions; Load-carrying cruciform joints; Strain energy density; Tension and bending.

1. Introduction

As one of the most typical connection types in shipbuilding or ocean engineering structures, the Load-carrying Cruciform Welded Joints (LCWJ) is widely used. The fatigue damage of these joints is a major threat for welded structures. When we assess the fatigue life of welded joints, the scatter of fatigue lives is affected intensively by joints geometry and loading modes for high cycle fatigue. Hence, it is critical to clarify the relationship among the geometry, cyclic loading and fatigue life. Many advanced local approaches have been proposed to characterize the fatigue life of welded joints, such as notch stress[1], hot spot stress[2], equivalent structural stress method[3], NSIF method[4, 5], SED method[6-8], peak stress method[9-11], fracture mechanics method[12], et al[13]. Although these methods avoid the influence of notch tip singularity at weld toe or weld root in weld components effectively, it still does not eliminate the process of establishing corresponding finite element models, especially for some typical welded joints. It drives the need for a more convenient predicted method for local fatigue characteristic values, which incorporates various factors about joints geometry and cyclic loading modes.

The nominal stress approach (S-N curves) is the most direct method for fatigue assessment of welded structures, which has been recommended in different welding standards[2]. Whereas the global stress-based

approach does not consider the local details geometrical variation surrounding the welded joints. Meanwhile, the analysis of local stress distribution based on stress, SED-related, and fracture mechanics methods needs extremely refined meshes or special mesh sizes due to the existence of stress singularity at sharp notch tip. It has limited the development of them toward complicated and large welded structures. SED method and peak stress method extended from NSIF method are widely adopted to assess uniaxial or multiaxial fatigue life of welded joints using a coarse mesh [14-20]. These methods have also been verified effectively for mixed loading brittle fracture and creep fracture for some notch components[21-24]. On the other hand, the fictitious notch rounding concept is also alternative method dealing with notch singularity issues[25, 26]. For the welding structures, the effective notch stress is typically obtained using finite element models with the reference radius of 1mm at sharp notches. Corresponding effective notch stress-based design class (FAT225) is derived from experiments for uniaxial and multiaxial fatigue strength assessment[27, 28]. Recently, fatigue life assessment of welded joints considering residual stress and material properties based on fictitious notch rounding concept are conducted by some researchers[29, 30].

Considering inherent variability of weld throat size and penetration size in LCWJ, the fatigue life of the weld toe failure tends to take significantly longer than weld root failure. Different from non-load-carrying cruciform welded joints (NLCWJ), plate thickness has a small influence on the fatigue strength of LCWJ [31]. Generally, fatigue crack initiated from weld toe in NLCWJ is governed by stress concentration, which is strongly related to plate thickness. Whereas fatigue crack originated from weld root in LCWJ is dependent on initial crack size. Different assumptions of initial crack sizes and crack types in welded cruciform joints were proposed and discussed according to corresponding fatigue performances by Zong[32]. Consequently, the 0.5mm weld toe line crack and 0.1 mm weld root initial line crack demonstrated a suitable fatigue life prediction compared with experimental results. To determine fatigue failure mode transition criteria between weld toe and weld root in LCWJ, Xing[33] employed Effective Traction Stress (ETS) and Equivalent Effective Traction Stress (EETS) to illustrate the relationship with variations of fillet weld size and penetration length. NSIFs are adequate to precisely describe the fatigue crack initiation at sharp corner notches or crack-liked notches [34]. Hence, it becomes possible that the SED method based on NSIF theory [35] is effective to examine the failure transition relationship between weld toe and weld root. Some local geometrical investigations in LCWJ under tension loading by local approaches or fracture mechanics approach, such as plate thickness[36, 37], weld shapes[31], angle or axial misalignment[32, 38], also have been conducted by researchers.

Although non-linear Finite Element Analysis (FEA) techniques are capable of calculating highly accurate

local stress, strain, NSIF, SED and other fatigue life indicators under arbitrary loading conditions, the process is computationally expensive and highly impractical for complex component geometries and/or long loading histories. The analytical formulations for fatigue assessment based on SED approach can estimate strain energy density at weld toe or weld root in LCWJ. From this perspective, some researchers have established some analytical solutions for different joints. Qian et al.[39] provided explicit parametric expressions for non-load-carrying fillet welded joints under tension, three-points, four-points bending loading conditions based on a volume-based hot-spot energy method. The results showed that it reduces the scatter in the high-cycle fatigue lives of welded plate joints compared to the existing structural stress methods. Saiprasertkit et al.[40] conducted high/low cycle fatigue experiments and numerical simulations to assess the fatigue performance comprehensively considering the material properties and joints geometries in LCWJ. Meanwhile, the corresponding low cycle fatigue analytical solutions incorporating material heterogeneity and geometry variations was also proposed extending the elastic fracture mechanics theory by effective notch strain method[41]. In addition, some fatigue designs of metallic components made by advanced manufacturing processing were evaluated according to local stress or energy method[42-45]. SED analytical solutions for NLCWJ can be obtained from NSIF analytical solutions proposed by Livieri[46], it still lacks some analytical solutions to calculate SED values rapidly for different failure modes in LCWJ under different loading conditions. Hence, these analytical researches give us some inspiration to deduce corresponding functions by SED results from FEA.

The primary goal is to develop analytical solutions for estimation of the averaged SED both at the weld toe and weld root in LCWJ. Firstly, we illustrate the fatigue characteristic parameters at weld toe and weld root based on NSIF and SED theories. Then taking some geometrical factors and cyclic loading conditions in LCWJ into account, the parameters will be calculated from the SED values using the finite element computation. The analytical equations under tension and bending conditions are further established. Subsequently, FEA is performed to confirm the validity of the formulation method by NSIFs and SED values. Additionally, weld toe angle is further incorporated into the analytical solutions. The evolution of fatigue transition boundaries is evaluated by the extended functions. Finally, the analytical solutions are converted to SED, NSIFs and peak stress range to assess several fatigue experimental results for weld toe and weld root failures in LCWJ.

2. Model description

2.1 SED analytical theory

The problem of singularity at sharp notch tip has been solved by Williams solutions for mode I and mode II loading. It involves different notch opening angles 2α to quantify the singularity by the following equations:

$$\sin(\lambda_1 q\pi) + \lambda_1 \sin(q\pi) = 0 \tag{1}$$

$$\sin(\lambda_2 q\pi) - \lambda_2 \sin(q\pi) = 0 \tag{2}$$

where q is related to the opening angle by the expression $2\alpha = \pi(2-q)$.

Lately, this solutions were introduced into the notch stress intensity factors, NSIFs, to characterize quantitively the intensity of the asymptotic stress distributions close to a notch tip using a polar coordinate system (r, θ). NSIFs related to Mode I and Mode II can be expressed by the notch stress fields, which are defined as follow equations[47]:

$$K_1^N = \sqrt{2\pi} \lim_{r\to 0^+} r^{1-\lambda_1} \sigma_{\theta\theta}(r, \theta = 0) \tag{3}$$

$$K_2^N = \sqrt{2\pi} \lim_{r\to 0^+} r^{1-\lambda_2} \tau_{r\theta}(r, \theta = 0) \tag{4}$$

where the stress components $\sigma_{\theta\theta}$ and $\sigma_{r\theta}$ have to be evaluated along the notch bisector (θ=0).

Due to the need for refined mesh strategy around the notch tip using NSIF method, it limited the development of this method toward complicated and large welded structures. For the sake of the advent of SED method, we can obtain the notch intensity conveniently and avoid the disadvantage of NSIF method that their units are not uniform for different notch angles. Under plane strain conditions, the SED solutions containing mode I and mode II can be expressed by Eq. (5) over a semicircular sector in Fig. 1[48].

$$\Delta\bar{W} = \frac{e_1}{E}\left[\frac{\Delta K_1^N}{R_c^{1-\lambda_1}}\right]^2 + \frac{e_2}{E}\left[\frac{\Delta K_2^N}{R_c^{1-\lambda_2}}\right]^2 \tag{5}$$

where E is the Young's modulus, R_c is the radius of the semicircular sector, which is dependent on the material properties. It is often defined as $R_c = 0.28mm$ for steel welded joints. e_1, e_2 are the parameters dependent on the opening angle, 2α and on the Poisson's ratio ν. A rapid calculation can be made for e_1 and e_2 from the following empirical equations[48]:

$$e_1 = -5.373\times10^{-6}(2\alpha)^2 + 6.151\times10^{-4}(2\alpha) + 0.1330 \tag{6}$$

$$e_2 = 4.809\times10^{-6}(2\alpha)^2 - 2.346\times10^{-4}(2\alpha) + 0.3400 \tag{7}$$

To simplify the expression of NSIFs based on the Williams formula, Lazzarin defined following convenient functions to assess the high cycle fatigue of welded joints for two fracture modes:

$$\Delta K_1^N = k_1 \Delta\sigma_n t^{1-\lambda_1} \tag{8}$$

$$\Delta K_2^N = k_2 \Delta\sigma_n t^{1-\lambda_2} \tag{9}$$

where $\Delta\sigma_n$ is the range of the remotely applied stress (nominal stress), t is the plate thickness and k_i are non-dimensional coefficients, which depend on the overall joint geometry and on the kind of remote applied load (membrane or bending). It provides a possible to realize the analytical expression for notch specimens. Furthermore, the SED equation can be rewritten as the following form from Eq. 5:

$$\Delta\bar{W} = \frac{\Delta\sigma_n^2}{E}\left[e_1 k_1^2 \left(\frac{t}{R_0}\right)^{2(1-\lambda_1)} + e_2 k_2^2 \left(\frac{t}{R_0}\right)^{2(1-\lambda_2)}\right] \tag{10}$$

Since it is complicated to calculate the non-dimensional coefficients, k_i by fine meshes near the notch tip, we should shift another way to obtain the corresponding formula for SED simplified expression. In the reference [49], the special parameter w_i linked to k_i was proposed to establish the SED analytical solutions of weld toe and weld root in the case of fully incomplete penetration in LCWJ[49]. However, these solutions do not consider penetration variations of weld fusion, that is the key parameter for fatigue failure assessment of weld root. Thus, it cannot illustrate the fatigue failure transition relationship between weld toe and weld root in CLWJ. Inspiration from the idea, the SED analytical solutions for weld toe and weld root in CLWJ also can be established considering the penetration effect by linking nominal stress components with another parameter K_i^*, which is similar with w_i. Then the following three non-dimensional parameters K_i^* are defined:

$$K_1^* = e_1 k_1^2 \tag{11}$$

$$K_2^* = e_2 k_2^2 \tag{12}$$

$$K_{eq}^* = K_1^* + K_2^* \tag{13}$$

where K_1^* , K_2^* and K_{eq}^* are non-dimensional parameters, conceptually equivalent to k_i parameters, except for the further dependence on the notch opening angle and the Poisson's ratio. Therefore, the Eq. 10 for SED can be rewritten by introducing the non-dimensional parameters K_i^*, which is used to explain the capability of local stress concentration, as follows:

$$\Delta\bar{W} = \frac{\Delta\sigma_n^2}{E}\left[K_1^*\left(\frac{t}{R_0}\right)^{2(1-\lambda_1)} + K_2^*\left(\frac{t}{R_0}\right)^{2(1-\lambda_2)}\right] \tag{14}$$

dealing with weld toe (135°) and weld root, it can be shown as two different expressions, respectively:

$$\Delta\bar{W}_{toe} = \frac{\Delta\sigma_n^2 \cdot K_1^*}{E}\left(\frac{t}{R_0}\right)^{2(1-\lambda_1)} \tag{15}$$

$$\Delta\bar{W}_{root} = \frac{\Delta\sigma_n^2 \cdot K_{eq}^*}{E}\left(\frac{t}{R_0}\right) \tag{16}$$

Finally, we can employ these functions to deduce analytical solutions of the non-dimensional parameters K_i^* from finite element analysis by using SED method.

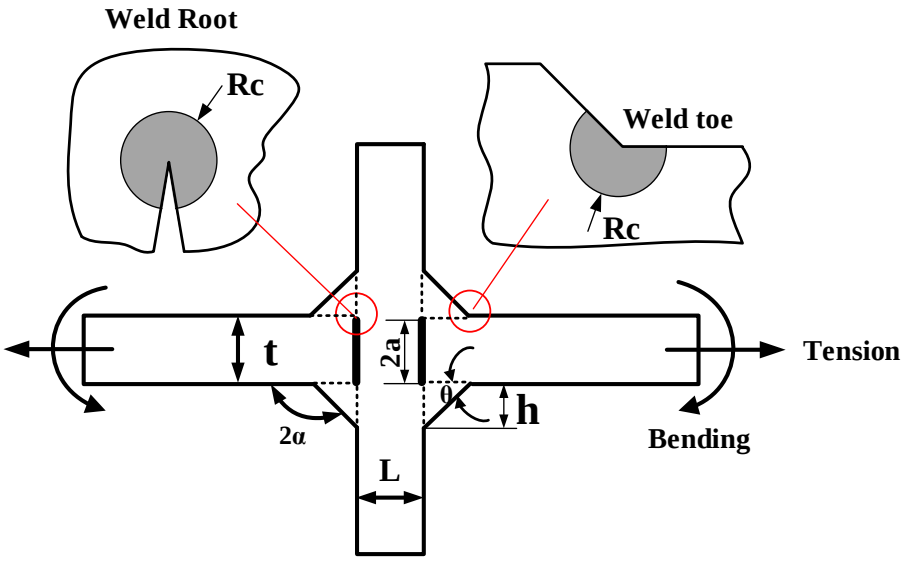

Fig. 1. Schematic Geometry of cruciform welded joints and corresponding SED geometry illustration.

2.2 Load-carrying cruciform welded joints models

As shown in Fig. 1, a typical LCWJ with a corner angle for the weld toe and 0° for the weld root crack under pure tension or bending loading were used for analysis in this study. The geometrical parameters in this type of welded joints were plate thickness *t*, attachment plate thickness designated by *L*, *h* stood for the

weld size, and 2*a* represented the crack length, which was dependent on the lack of penetration *p*. All LCWJ models were conducted to calculate and infer analytical solutions of the non-dimensional parameters K_i^* using FEM. A representative quarter part and half part of the 2D LCWJ were modeled under axial tensile and bending loading (100MPa) respectively, which is shown in Fig. 2. Additionally, it is worth mentioning that the bending force is loaded to the upper and lower halves of the nominal cross-section, respectively. This special setting can meet the final demand for bending loading.

Abaqus 6.14 was employed for the numerical analyses and two distinct boundary conditions were considered in LCWJ for the tension and bending loading conditions according to geometrical symmetry. In the elastic mechanics' regime, the material properties of base metal and weldments are assumed to be homogeneous and isotropic. The Poisson's ratio was ν=0.3 and Young's modulus was E=206 GPa for steel and these values were used for all FE models.

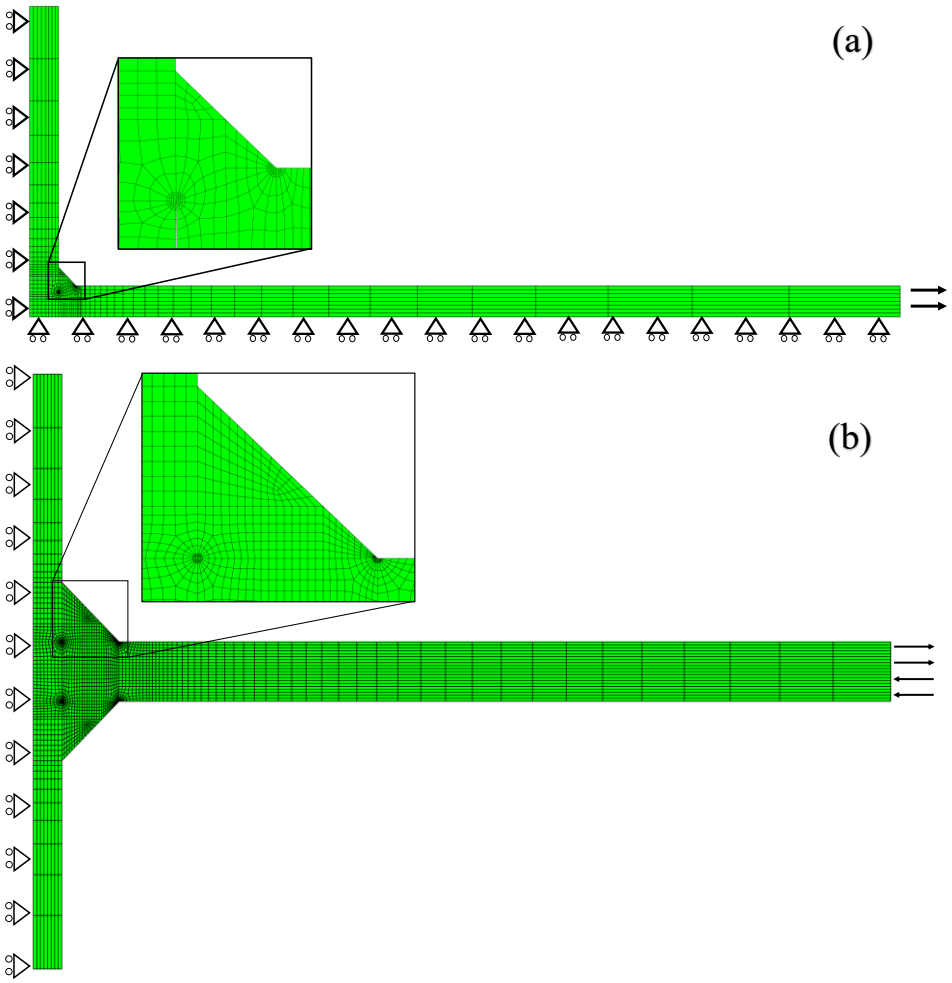

Fig. 2. Illustrations of LCWJ models showing finite element mesh and boundary conditions under different loading conditions. (a) tension loading (1/4 model), (b) bending loading (1/2 model).

3. The analytical equation based on SED method

In order to drive analytical solutions of SED evolution for weld toe and weld root, the following assumptions are made: (a) Geometry of welded joints are assumed as ideal without any defeats, such as axial or angular misalignment and pores, since the additional stress concentration effect needs be considered. (b) Given the generality of analytical results, the implicit gradient effect near free surface for LCWJ 3D models were not included into solutions. SED values from FE simulations were obtained firstly by the variations of joints geometric parameters under pure tension and bending loading, such as plate thickness, weld length, weld penetration. Then the corresponding non-dimensional parameters, K_i^* were generated. The analytical solutions were deduced from these results. In what follows, a series of numerical results of NSIFs and SED values are presented to demonstrate the effectiveness of the proposed analytical functions. Furthermore, the equations are extended taking the effect of load-carrying weld angle into accounts.

3.1 Geometrical effects on weld toe and root in LCWJ

In order to infer the analytical equations of LCWJ accurately under tension and bending loading, each geometrical effort on the non-dimensional parameters, K_i^* should be considered. Firstly, the attachment plate thickness effect on K_1^* and K_{eq}^* is considered under pure tension and bending loading conditions in a wide range of *h/t* and *L/t*, which is expressed in Fig. 3. It can be seen that K_1^* for weld toe rapidly decreases with the increases of weld length ratio (*h/t*), while the *L/t* shows a negligible effect on these values independent of loading conditions. It is worthy to note that the non-dimensional parameters K_i^* under tension loading are always higher than that under bending loading. It is the same case for the non-dimensional parameter K_{eq}^* with all the combination of *p/t* and *h/t* in the range of interest, as shown in Fig. 3(b). Therefore, the attachment plate thickness effect on the fatigue capacity of LCWJ is not considered for design evaluation purpose under different loading conditions.

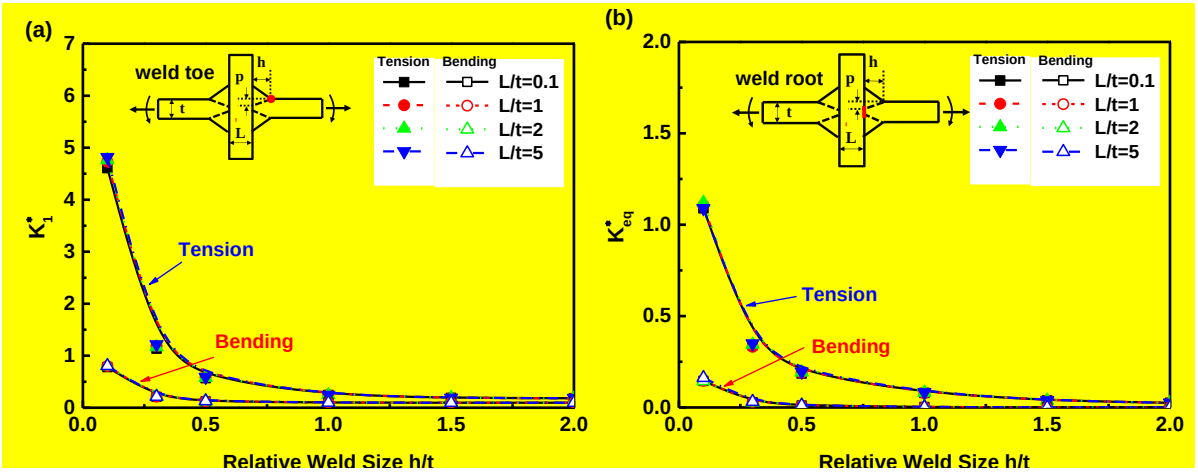

Fig. 3. K_1^* (a) and K_{eq}^* (b) variations in LCWJs under pure tension and pure bending loading.

As shown in Fig. 4, as the penetration ratio (p/t) increases from 0 to 0.4, the K_1^* and K_{eq}^* extracted from SED values at weld toe decreases significantly as p/t increases. On the other hand, the penetration ratio (p/t) effect on the K_1^* and K_{eq}^* values under bending loading is shown in Fig. 4(c)-(d). It can be seen from this figure that the values of K_i^* have slight effects by the penetration ratio (p/t) when the h/t is in the range from 0.5 to 2. Whereas, there is some difference in the range from 0.3-0.5. The weld penetration shows a significant effect on fatigue parameter SED values at weld toe and weld root.

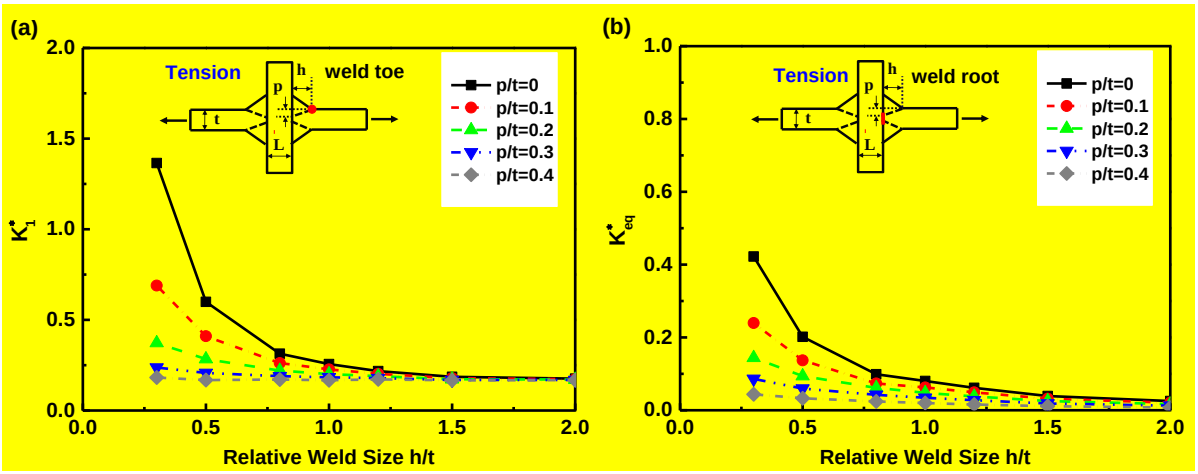

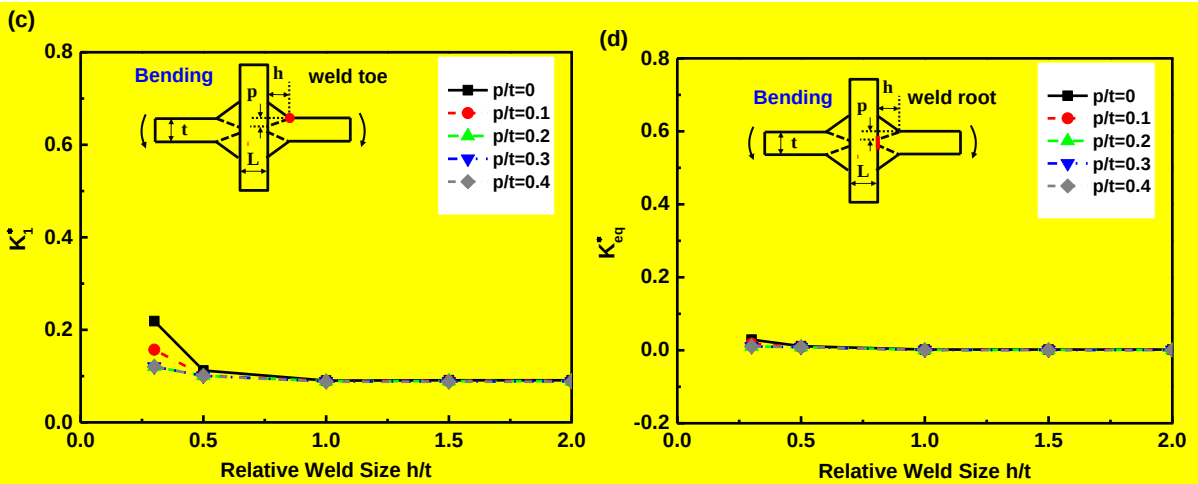

Fig. 4. K_1^* (weld toe) and K_{eq}^* (weld root) variations in LCWJ under tension and bending loading.

3.2 Determination of analytical solutions

Considering the comprehensive effects of geometric parameters on the non-dimensional parameters K_i^* that was discussed above, we can deduce the analytical equations for the curves in Fig. 4 via least square fitting. Lazzarin et al. [5] and Atzori et al.[50] have proposed some expressions for non-dimensional parameters k_i from notch stress intensity factor in non-load-carrying cruciform joints under pure tension:

$$k_1 = 1.212 + 0.495e^{-0.985(2b/t)} - 1.259e^{-1.12(2b/t)-0.485(t'/t)} \tag{17}$$

$$k_2 = 0.508 - 0.797e^{-1.959(2b/t)} + 2.723e^{-1.126(2b/t)-0.769(t'/t)} \tag{18}$$

Similar to the function form of k_i, the equations of non-dimensional parameters K_i^* for LCWJ under pure tension and bending loadings can be shown as follows:

$$K_i^* = \left[A_i + B_i \cdot e^{\alpha_i (h/t)} + C_i \cdot e^{\beta_i (h/t) + \gamma_i (p/t)} \right]^2 \tag{19}$$

The numerical analyses of LCWJ under different loading conditions demonstrate local geometry imposes negligible effect on the strain energy density, as also reflects in Eq. (19), which does not include the dependence on the attachment plate thickness (L) while incorporates the effects of weld length (h) and penetration length (p). These parameters are obtained from the least square method for model interest in this study. Finally, the K_i^* equations of weld toe and weld root under different loading conditions from the Eq. (19) becomes:

For weld toe:

Tension: $$K_1^* = \left[0.4135 - 0.4404 \cdot e^{-3.685(h/t)} + 2.334 \cdot e^{-3.174(h/t)-4.707(p/t)}\right]^2 \quad (20)$$

Bending: $$K_1^* = \left[0.2959 + 0.1886 \cdot e^{-5.043(h/t)} + 1.878 \cdot e^{-8.932(h/t)-9.643(p/t)}\right]^2 \quad (21)$$

For weld root:

Tension: $$K_{eq}^* = \left[0.1377 - 0.534 \cdot e^{-1.817(h/t)} + 1.368 \cdot e^{-1.773(h/t)-1.801(p/t)}\right]^2 \quad (22)$$

Bending: $$K_{eq}^* = \left[0.0258 + 0.1272 \cdot e^{-1.762(h/t)} + 0.2746 \cdot e^{-4.552(h/t)-8.111(p/t)}\right]^2 \quad (23)$$

Based on these equations, the SED values at weld toe or weld root in LCWJ can be simply estimated without doing any finite element analysis. The verifications of these functions are conducted in the next section.

3.3 Angle effect on K_i^*

The above proposed equations are evidently insufficient to calculate the SED values for different weld shape in LCWJ. In general, the fatigue study on LCWJ is focused on the isosceles-triangle-shaped fillet welds. However, weld shape has some influence on the determination of SED values. The weld shape is often dependent on the welding position and welding conditions. Kainuma et al. [31] investigated the fatigue strength of LCWJ considering the five types of weld shape according to the flank angle at weld toe. The isosceles-triangle-shaped welds are defined as θ=135°. Then, the concave welds and convex welds stand for the cases of θ>135° and θ<135°, respectively. The results showed that the fatigue strength of the joints with concave or convex welds was greater than the fatigue strength of the joints with the isosceles-triangle-shaped welds. As the flank angle (θ) at weld toe in LCWJ has a great influence on the accuracy of SED values, the equations should incorporate it into the SED predicted functions.

The same finite element model is employed as before. Given some geometry parameters are kept constant, the attachment plate thickness (L) has little influence on non-dimensional parameters K_i^*. Therefore, only three variables are considered to calculate SED values for all cases. For a given combination of p/t and flank angle (θ), the values of h/t can exert a significant influence on K_1^* under tension loading, see from Fig. 5(a)-(c). The values K_1^* of weld toe become smaller with increases of flank angle (θ) for different weld penetration to weld plate ratios (p/t). Whereas K_{eq}^* of weld root nearly remain same values for different

p/t ratios in Fig. 5(d)-(f). It is further demonstrated that the flank angle effects can be included in the weld toe analytical solutions, and the weld root functions are not varied for the estimation of SED results. Due to the negligible SED values at weld root under bending, the target of SED analytical solutions is focused on the weld toe. Similar to pure tension condition, the values K_1^* show slightly decreases for the increases of flank angles at weld toe under pure bending.

So far, the effects of all effects *h/t*, *p/t*, flank angle (θ), and loading mode have been taken into account in SED results. We further enrich Eq. 19 from above analysis via least square fitting. The predicted equations for weld toe are summarized as follows for pure tension and bending loading:

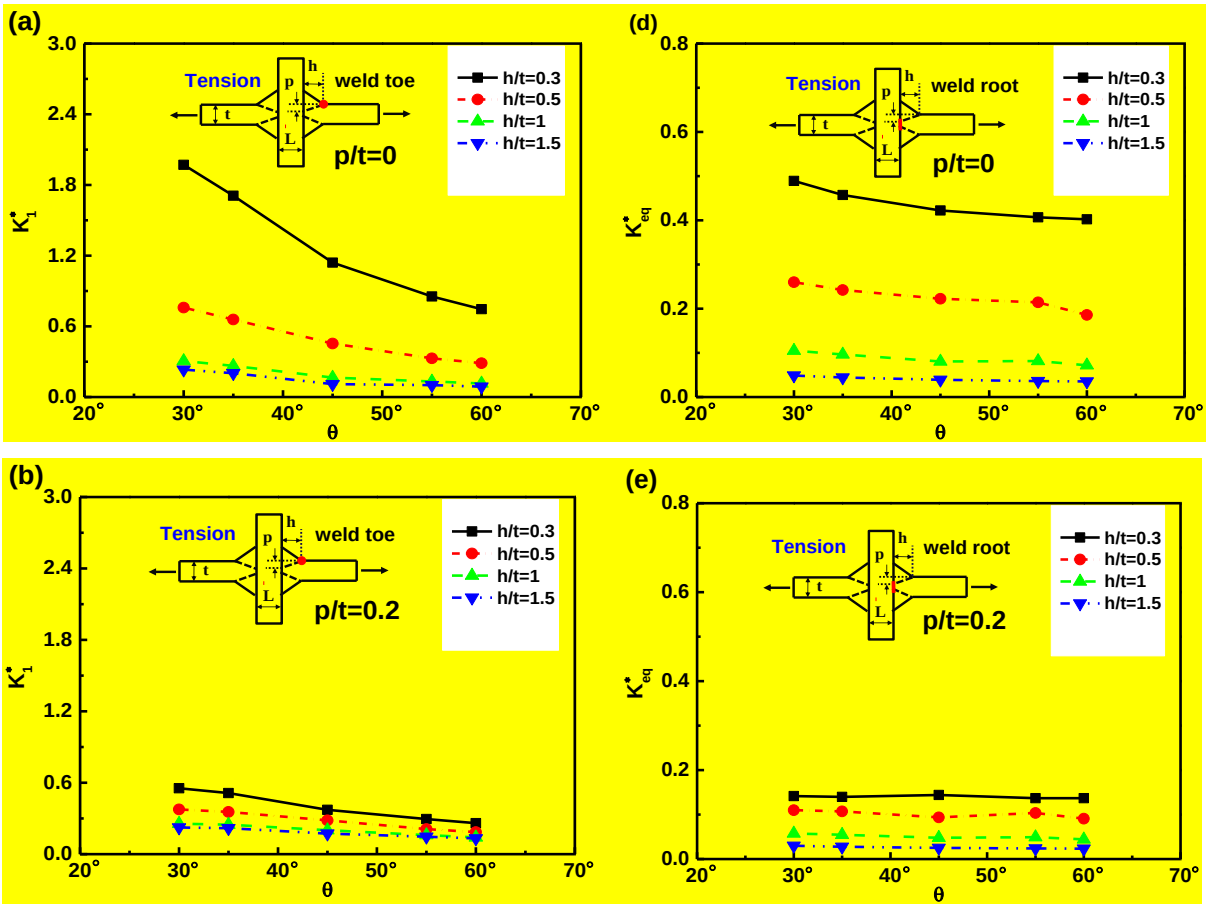

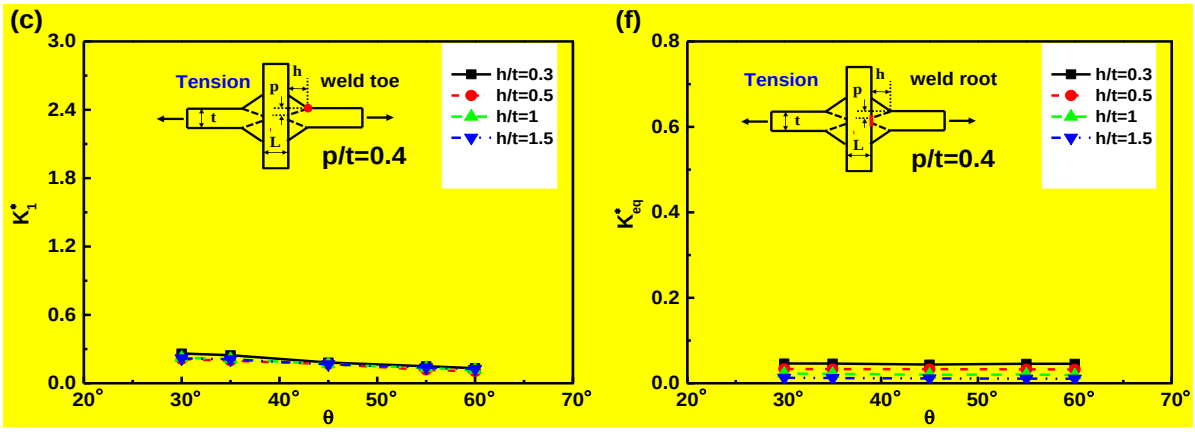

Fig. 5. K_1^* (weld toe) and K_{eq}^* (weld root) variations in LCWJ under pure tension considering different penetration lengths.

For weld toe under pure tension:

$$A(\theta) = -0.0032 * \theta + 0.55487 \tag{24}$$

$$B(\theta) = 0.0054 * \theta^2 - 0.454 * \theta + 5.768 \tag{25}$$

$$C(\theta) = 9.87 * \theta^2 - 0.086 * \theta + 1.46 \tag{26}$$

$$\alpha(\theta) = 0.036 * \theta^2 - 0.343 * \theta + 10.37 \tag{27}$$

$$\beta(\theta) = -0.0057 * \theta^2 + 0.4757 * \theta - 13.2 \tag{28}$$

$$\gamma(\theta) = 0.037 * \theta - 6.346 \tag{29}$$

For weld toe under pure bending:

$$A(\theta) = -0.0038 * \theta + 0.4875 \tag{30}$$

$$B(\theta) = 0.02 * \theta - 0.068 \tag{31}$$

$$C(\theta) = -0.0027 * \theta^2 + 0.242 * \theta - 3.7 \tag{32}$$

$$\alpha(\theta) = -0.007 * \theta^2 - 0.447 * \theta - 10.76 \tag{33}$$

$$\beta(\theta) = 0.0095 * \theta^2 - 0.8877 * \theta - 12.19 \tag{34}$$

$$\gamma(\theta) = -0.163 * \theta - 2.115 \tag{35}$$

3.4 Verification of analytical equations

The solutions for LCWJ are further validated by different numerical results based on NSIFs and SEDs for the flank angle 45°. Firstly, the comparison between analytical results and NSIFs from FE simulations under tension loading are given in Fig. 6. It is shown that the analytical solutions of weld toe give a very good prediction of the NSIFs for the p/t range from 0.1 to 0.4, while the results from the proposed equation slightly overestimate NSIF values for p/t=0. It is because that the SED values are governed by the intensity combination of K_1^*, K_2^*. When weld penetration decreases, it leads to the increasing of bending degree and further makes the SED values increase.

Fig. 7 depicts the comparisons between the predictions of the analytical model (Eq. 19) and the numerical results for SED values at weld toe and weld root under pure tension considering different p/t. Fig. 7(a) shows that good agreement has been achieved for the cases in the range from h/t=0 to h/t= 2 at weld toe under tension loading. Nearly all the numerical calculation data coincide with the analytical predicted lines for p/t in the range from 0 to 0.4. Especially, there is an excellent agreement between the estimated results and numerical calculation results for the cases that p/t is equal to 0.1 to 0.4. The similar results can be observed at weld root from the Fig. 7(b). On the other hand, the SED predictions from the analytical model (Eq. 19) are still satisfactory with numerical calculation results under pure bending in Fig. 7(c)-(d). It should be noticed that the values in the cases that h/t is in the range between 0.5 to 2 demonstrate the same magnitudes. We note that as expected, the analytical solutions fit quite well the numerical results obtained for the physically SED values of weld toe and weld root. The proposed analytical equations are evidently sufficient to retrieve the SED values from numerical calculation results considering different geometry effects and loading conditions.

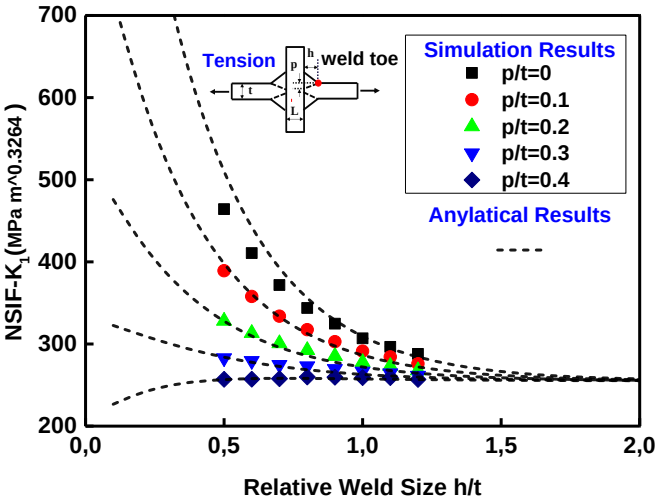

Fig. 6. Comparisons between the predictions of the analytical model (Eq. 19) and the numerical results for NSIFs in LCWJ under pure tension considering different *p/t*.

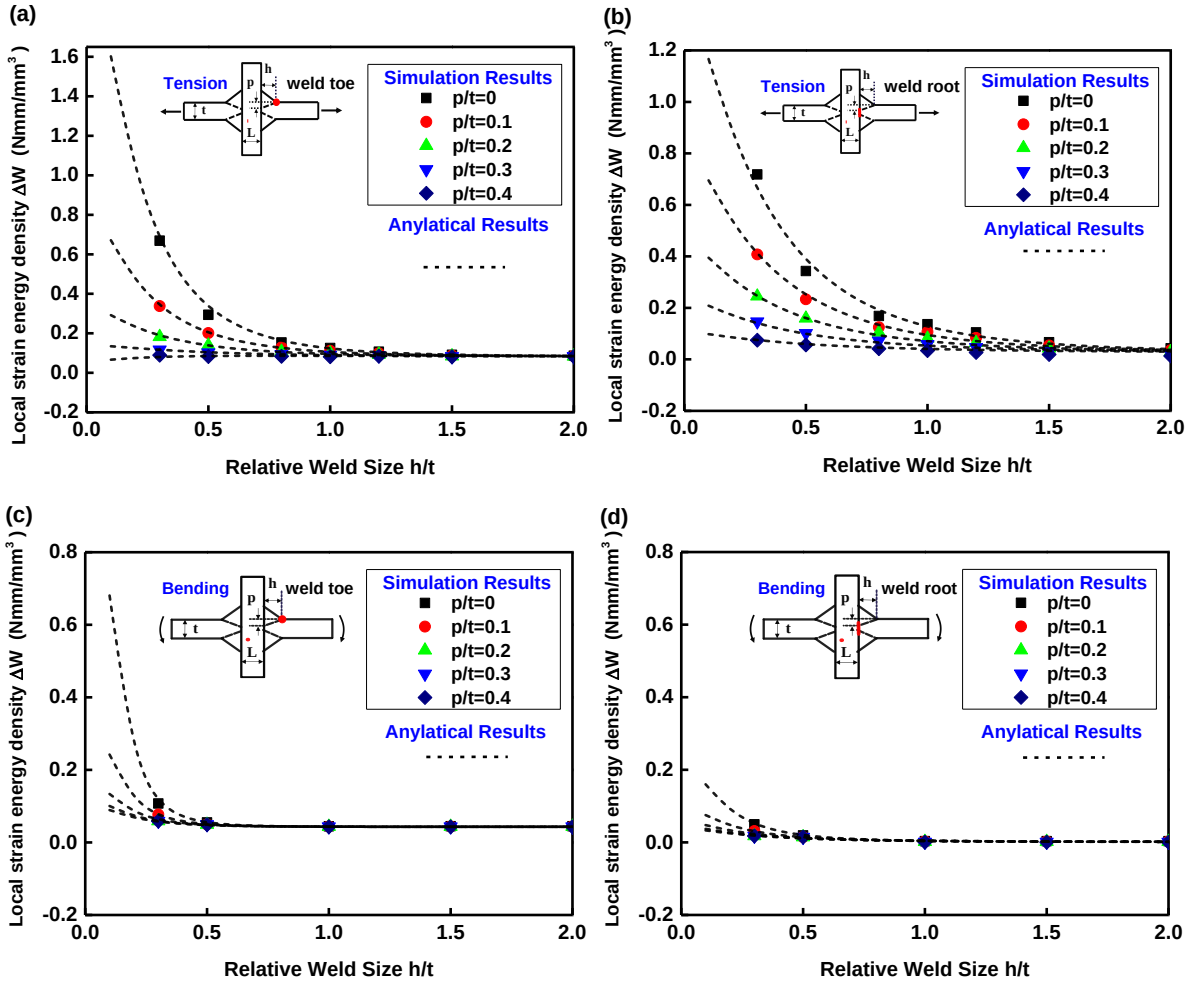

Fig. 7. Comparisons between the SED predictions (Eq. 19) and the numerical results at weld toe and weld root under pure tension and bending conditions considering different *p/t*.

3 The evolution of failure mode transition

In this section, weld toe and weld root failure in LCWJ are investigated based on the SED analytical solutions. The evolution of failure transition is analyzed according to local geometrical variations. Then the transition criterion based on SED method are proposed. Different failure mode transition criteria are compared with methods in the references [33], [51]. Similar with failure zone evolution for flank angle 45°, different flank angles are further investigated from the analytical equations.

4.1 Comparison of failure mode criteria at flank angle 45°

Fig. 8 plots failure transition zone prediction contour based on the SED analytical solutions under same tension loading at flank angle 45° in LCWJ. The green plane stands for weld toe SED values, and the blue plane presents weld root values in LCWJ. If weld toe value is higher than weld root value at same geometry, we identify the fatigue crack originated from the weld toe. In contrast, weld root failure occurs. Fig. 8(a) gives different SED variations at weld toe and weld root with the geometrical factors *h/t* and *p/t* by 3D contour. The discrepancy of SED decreasing trends exerts a significant effect on failure mode transition from weld root to weld toe with the increases of *h/t* and *p/t*. Fig. 8(b) depicts the transition zone according to the variations of *h/t* and *p/t* by 2D contour. The criterion of failure modes can be described clearly by the color contrast of weld toe plane and weld root plane in Fig. 8(b). The intersection line can be found with a different combination of *h/t* and *p/t*.

The comparisons of failure mode transition relationship between SED analytical solutions and other models in LCWJ is shown in Fig. 8(c). In this figure, the blue points stand for the criterion from SED method, the black points represent the Petershagen criterion[51] based on the notch stress approach, the brown points are the criterions from Dong's ETS and EETS methods[33], and the dash lines are the criterions proposed by Maddox[51] in terms of crack propagation approach. The corresponding curves of these criterions and their tendencies are similar. From the comparison between SED criterion and Petershagen criterion, it shows good agreement for the *p/t* range from 0 to 0.2, as shown in Fig. 15. While the area of weld root failure judged by SED criterion becomes smaller than the area judged by Petershagen criterion for *p/t* above 0.2. It means that the possibility of weld root based on SED criterion is higher than Petershagen criterion when *p/t* is over 0.2. Similarly, ETS criterion shows a narrow range

of weld root failure compared with that by EETS criterion. The difference of SED criterion in comparison to ETS and EETS criteria has been verified by experiments data in Ref. [35]. Different from the Maddox criterion for crack propagation approach, the failure zone transition curves from other criteria are independent of the length dimension. Another point should be highlighted that the main discrepancy lies on different failure performances. The former methods are related to crack initiation, but Maddox method focuses on the crack propagation, which is strongly dependent on the plate thickness. Considering joints with the varying weld length, weld penetration and plate thickness, the optimization of local geometrical factors can be conducted to realize weld toe failure. Therefore, SED criterion can be used to design the fillet joints to exclude root failures.

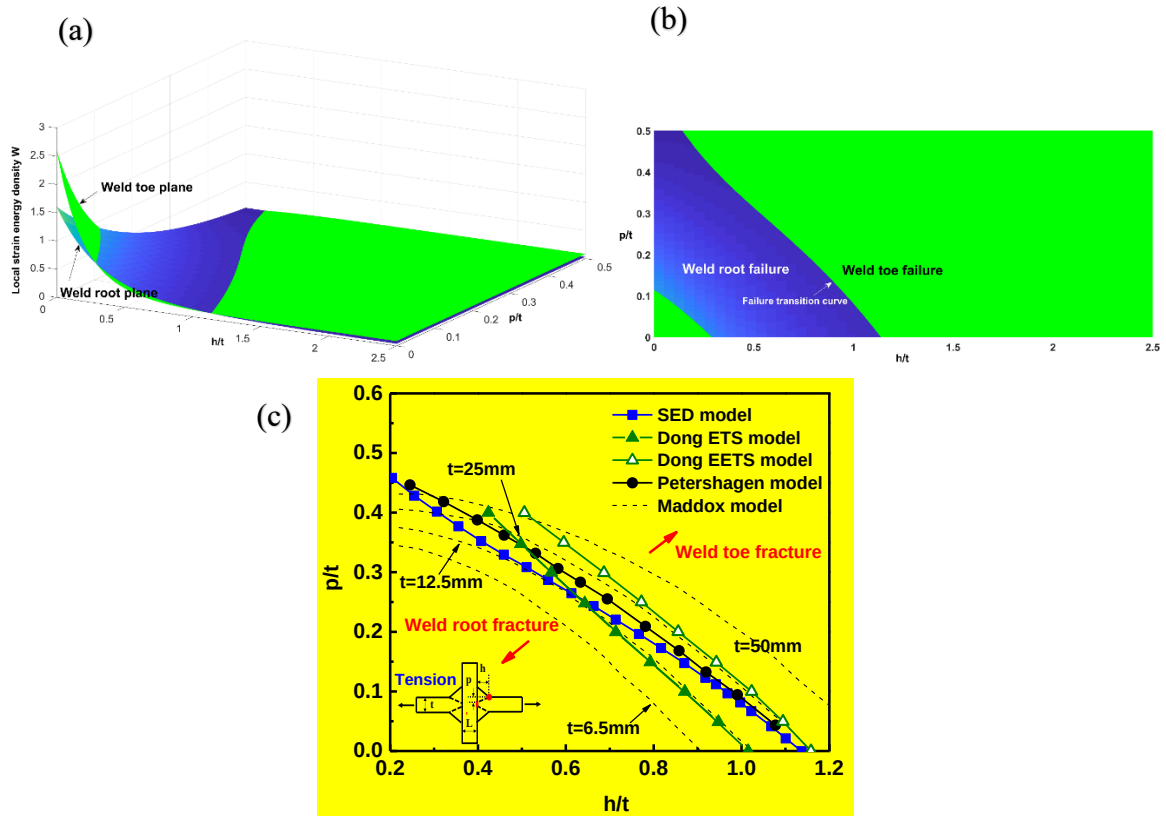

Fig. 8. Failure transition zone prediction based on the SED analytical solutions under tension at flank angle 45° (a) 3D; (b) 2D; and (c) different failure mode criteria for LCWJ.

4.2 The evolution of failure transition

The failure transition criterion based on SED method has been discussed by comparing the results with other criteria under pure tension loading in the last section. We can also use the proposed analytical equations

to analyze the evolution of failure transition zones under different flank angles. The selected values of flank angle are 30°, 35°, 45°, 55°, 60°. Fig. 9 shows the evolution contours of failure mode transition zone with different flank angles in LCWJ. The failure transition zone in LCWJ exhibits obvious flank angle dependence in the evolution of transition boundaries. The weld root zone shrinks with increasing the flank angle. Meanwhile, the boundary between weld root plane and weld toe plane is moved from the changing contours. In order to quantify the failure transition boundaries, the transition curves are portrayed according to weld root and weld toe boundaries in Fig. 10. The transition curves moved towards left with the increases of the flank angle from 30° to 45°. However, the curve returns to right side when the flank angle is over 45°. Therefore, the flank angle variation based on 45° can increase the possibility of weld root.

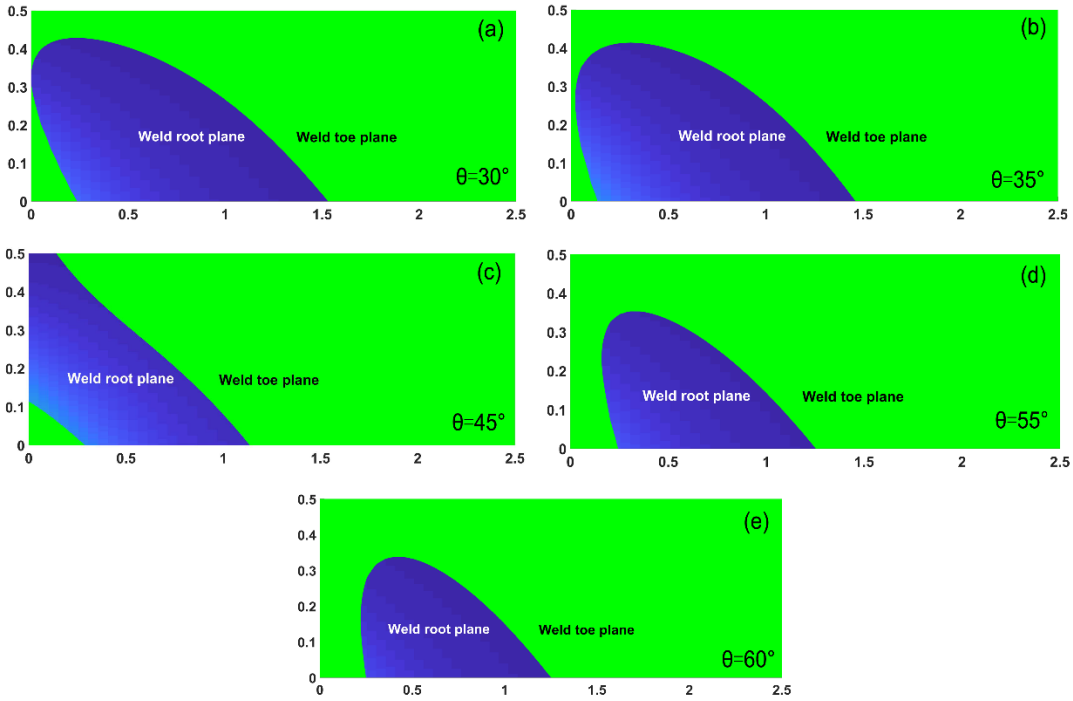

Fig. 9. The evolution of failure mode transition zone with different flank angles in LCWJ.

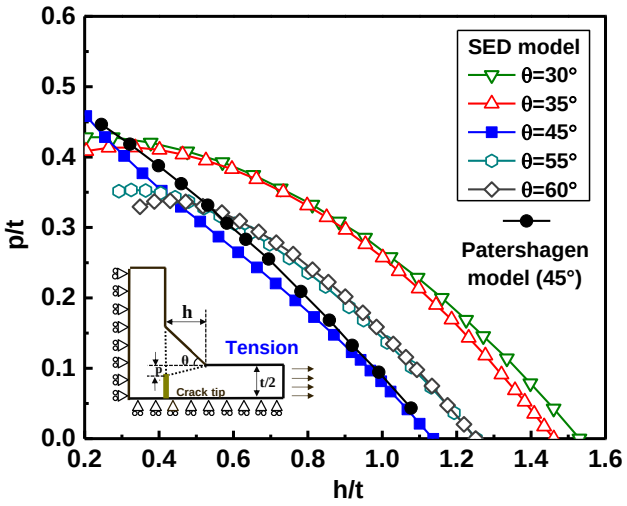

Fig. 10. Comparisons of failure mode transition relationship with different models in LCWJ.

4 Experimental verification

In this section, the experiments data were used to verify the proposed analytical solutions. High cycle fatigue experiments of load-carrying cruciform welded joints were performed on a 250KN electro-hydraulic servo testing system MTS 809 with a load-control condition. Fig. 11 illustrates the procedure of specimens processing and fatigue tests. Two panels of 10CrNi3MoV steel were fabricated in Fig. 11(a). Each panel was cut up into LCWJ specimens of 35mm width by wire-electrode method, as shown in Fig. 11(b). This steel yield stress is about 693MPa. The nominal stress range of 100-200 MPa was tested in the as-welded conditions with a stress ratio R=0.1 and loading frequency in the range from 5 to 15 Hz.

Before fatigue tests, the LCWJ geometrical profile obtained by image scanner were measured by CAD software. In order to determine each size of weldments in LCWJ, the weldments were classified into four regions, as W_1, W_2, W_3, W_4, as shown in Fig. 12(a)-(b). 24 specimens in total were measured and tested. It should be noted that the zero penetration at weld root is realized by wire-electrode method. The geometrical sizes of each specimens, fatigue test data and fatigue failure locations are summarized in Table 1. The typical weld toe and weld root failure modes obtained after fatigue tests are shown in Fig. 12(c). Due to the difference of weld penetration in LCWJ, the fatigue failure modes change according to the variation of penetration length at weld root.

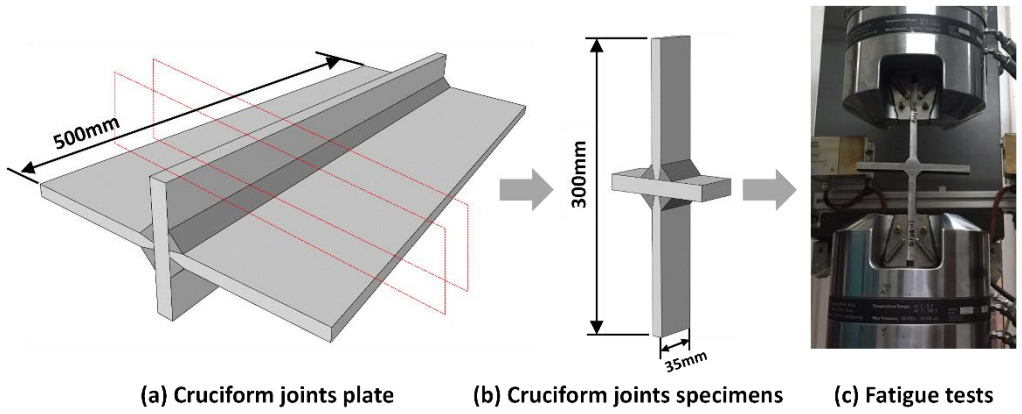

Fig. 11. Load-carrying cruciform plate/joints specimen sizes and fatigue tests.

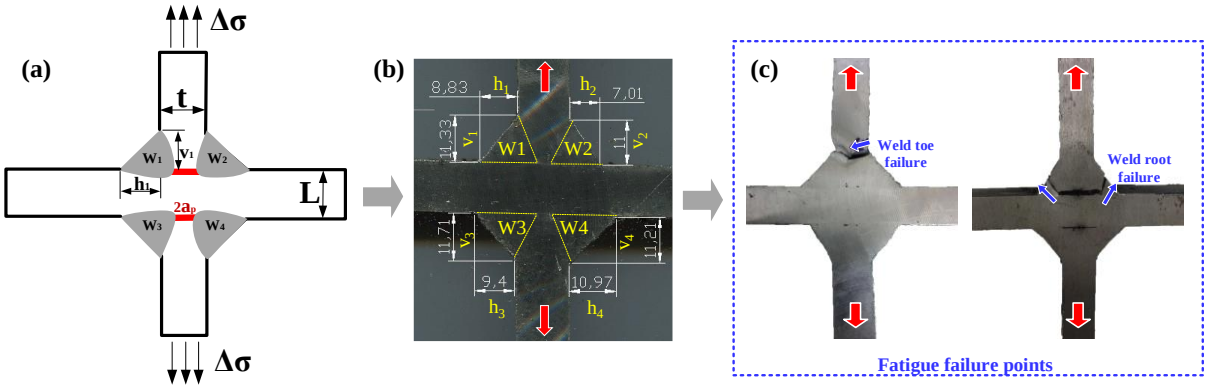

Fig. 12. The schemic specimen geometry and fatigue failure points for LCWJ.

Table 1. 10CrNi3MoV LCWJ geometry sizes, fatigue loading conditions and results.

Specimens	Weld$_1$ (mm)		Weld$_2$ (mm)		Weld$_3$ (mm)		Weld$_4$ (mm)		t mm	p/t	h/t(v/t)	Weld toe angle (θ)	Stress range (MPa)	Stress ratio	Fatigue life	Fracture location
	h_1	v_1	h_2	v_2	h_3	v_3	h_4	v_4								
Sp1	10.19	10.21	10.56	11.89	10.49	11.38	8.82	9.9	12	0.3	0.83	41.7	400	0.1	21500	Weld toe
Sp2	10.57	10.52	10.11	12.94	10.08	12.08	9.05	9.87	12	0.3	0.82	42.5	360	0.1	37800	Weld toe
Sp3	10.27	10.36	9.82	11.56	9.9	11.9	8.85	10.21	12	0.3	0.85	40.9	320	0.1	46800	Weld toe
Sp4	10.19	10.21	10.56	11.89	10.49	11.38	8.82	9.9	12	0.3	0.83	41.7	280	0.1	56580	Weld toe
Sp5	10.57	10.52	10.11	12.94	10.08	12.08	9.05	9.87	12	0.3	0.82	42.5	240	0.1	129600	Weld toe
Sp6	10.27	10.36	9.82	11.56	9.9	11.9	8.85	10.21	12	0.3	0.85	40.9	200	0.1	224700	Weld toe
Sp7	6.42	7.7	5.01	9.16	6.39	9.98	5.57	8.83	12	0.3	0.64	39.8	240	0.1	327400	Weld toe
Sp8	6.44	7.62	5.12	8.9	6.42	9.33	6.29	8.88	12	0.3	0.64	40.2	400	0.1	15200	Weld toe
Sp9	5.41	9.02	6.12	7.53	5.66	9.27	6.11	9.74	12	0.3	0.75	31.0	360	0.1	47000	Weld toe
Sp10	5.22	9.06	6.12	7.85	6.17	9.35	6.43	9.21	12	0.3	0.76	29.9	280	0.1	160700	Weld toe
Sp11	7.42	9.62	7.57	9.74	6.38	9.3	7.62	8.7	12	0.3	0.78	34.5	180	0.1	95000	Weld toe

Sp12	7.87	9.9	7.52	9.09	6.8	9.54	7.45	9.01	12	0.3	0.80	35.5	150	0.1	204100	Weld toe
Sp13	9.36	10.34	6.67	9.04	6.53	9.83	7.61	9.15	12	0.3	0.82	33.6	120	0.1	429300	Weld toe
Sp14	7.38	9.55	7.49	8.78	6.3	9.32	7.85	9.2	12	0.3	0.78	34.1	160	0.1	157400	Weld toe
Sp15	8.83	11.33	7.01	11	9.4	11.7	10.97	11.21	12	0,3	0.92	32.5	300	0.1	118800	Weld toe
Sp16	8.87	10.72	7.35	11.54	9.8	10.4	10.39	11.08	12	0,3	0.96	32.5	320	0.1	73200	Weld toe
Sp17	9.01	12	7.51	10.22	10.49	10.73	11.48	11.23	12	0,3	0.85	36.3	305	0.1	28700	Weld toe
Sp18	8.89	12.33	6.91	10.94	10.49	11.1	10.8	11.93	12	0,3	0.91	32.3	305	0.1	53500	Weld toe
Sp19	8.13	8.52	7.25	8.6	8.5	8.62	7.8	9.63	12	0	0.72	34.4	100	0.1	320500	Weld root
Sp20	8.12	9.43	8.22	8.95	9.22	8.17	8.54	7	12	0	0.68	35.2	120	0.1	184500	Weld root
Sp21	6.85	8.24	6.55	8.78	6.1	8.06	7.72	8.28	12	0	0.67	37.1	120	0.1	156900	Weld root
Sp22	8.15	9.49	8.53	8.95	9.22	8.17	8.54	10	12	0	0.68	45.5	150	0.1	41400	Weld root
Sp23	8.16	8.33	6.06	7.86	6.02	8.62	7.8	9.63	12	0	0.72	34.9	150	0.1	54190	Weld root
Sp24	7.16	8.5	6.32	8.68	5.2	7.64	7.82	8.32	12	0	0.64	34.2	180	0.1	75450	Weld root

Fig. 13(a) shows fatigue test results of 10CrNi3MoV LCWJ expressed in terms of nominal stress range. According to IIW standard, the fatigue strength of weld toe failure for LCWJ is higher than weld root failure. The FAT of weld toe and weld root in LCWJ are 63 and 36, respectively. The slope of these lines is fixed as 3 in terms of steel. It also illustrates that the fatigue strength of weld root failure is lower than weld toe failure. It proved that the design curves of IIW were suitable for the experimental data. Fig. 13(b) compares the experimental data relevant to LCWJ made of 10CrNi3MoV steel with the SED fatigue scatter band suggested to design steel welded joints. The proposal formulated by Lazzarin [52] was adopted here. In this figure, the design scatter bond was proposed by fitting approximately 200 experimental data taken from literatures. The fatigue strength expressed by averaged strain energy density is $\Delta W_{50\%}$=0.015 N mm/mm^3, and the inverse slope of the design scatter band is 1.5. The maximum flank angle and minimum weld length were chosen to estimate the SED values for fatigue assessment. Therefore, the predicted SED values from analytical solutions shows good agreement with SED fatigue design scatter band for weld toe and weld root failure. Despite three experimental data is out of SED design scatter band, it can be illustrated that occasional fatigue failure may occur due to other factors, like initial crack depth variation between specimens, penetration length uncertainties, inner weld flaw, or secondary bending.

In order to illustrate the relationship between SED and peak stress method, Meneghetti[53] used the simple mesh-insensitive peak stress to deduce the closed-form expression of the averaged SED, which can be

written as follows:

$$\Delta\bar{W} = \frac{e_1}{E}\left[K_{FE}^{*}\cdot\Delta\sigma_{peak}\cdot\left(\frac{d}{R_0}\right)^{1-\lambda_1}\right]^2 = \frac{1-\upsilon^2}{2E}\Delta\sigma_{eq}^2 \tag{36}$$

The relationship between $\Delta\sigma_{peak}$ and $\Delta\sigma_{eq}$ can be linked by a correction parameter f_w, which is shown as follows:

$$f_w\cdot\Delta\sigma_{peak} = \Delta\sigma_{eq} \tag{37}$$

For the notch opening angle $2\alpha = 135°$, the parameter is obtained as 1.064. To further demonstrate the effectiveness of analytical solutions, these experimental data expressed in terms of nominal stress were converted in terms of range of NSIFs and peak stress according to Eq.5 and Eq. 36. The fatigue design scatter bands of NSIFs and peak stresses reported in reference [46] and [53] are valid for these experimental data by estimating the corresponding fatigue characteristic parameters. These design curves are effective for the fatigue strength assessments of welded joints failing from weld toe or weld root. Regarding the fatigue failure criterion based on SED, it shows clearly that the SED criterion boundary can be used to separate the failure mode for weld toe and weld root in LCWJ, see Fig. 14.

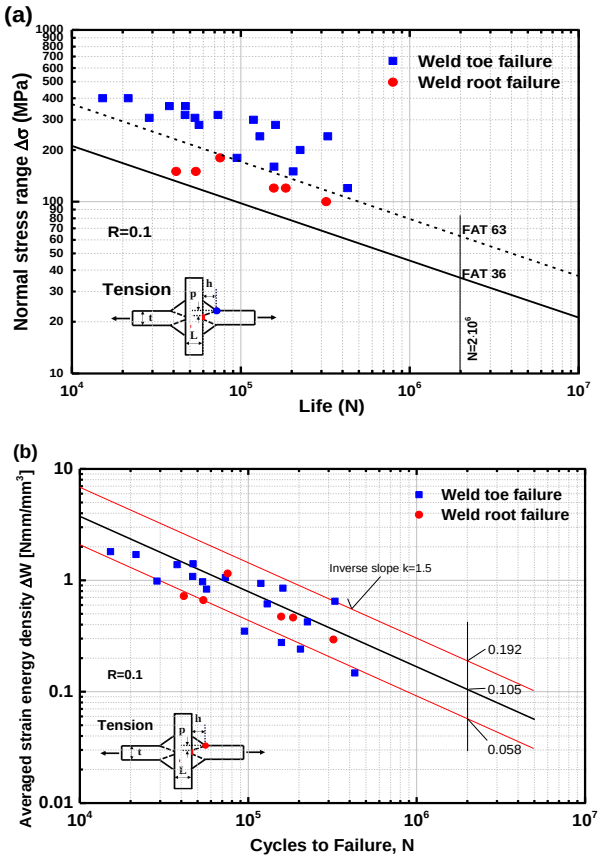

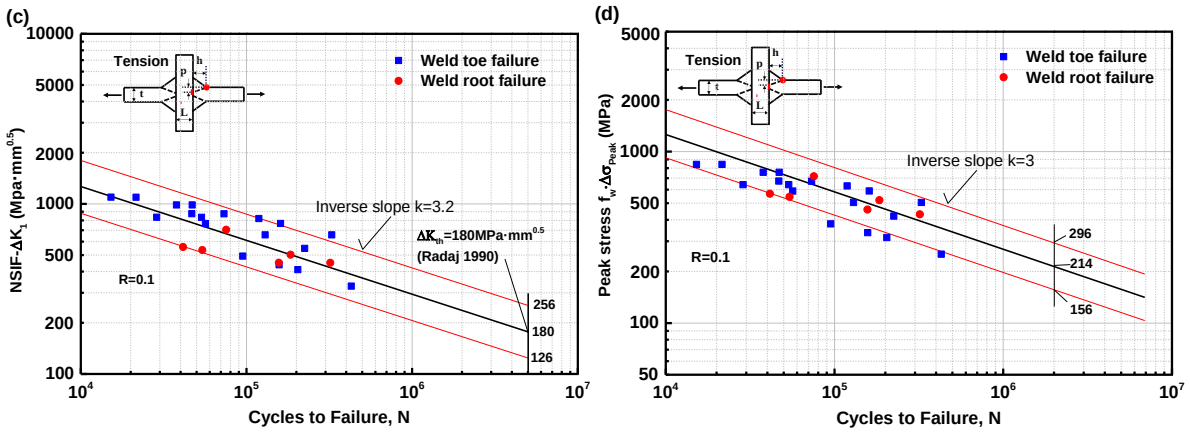

Fig. 13. Fatigue test results of 10CrNi3MoV LCWJ expressed in terms of nominal stress range, ΔW, N-SIF and peak stress method.

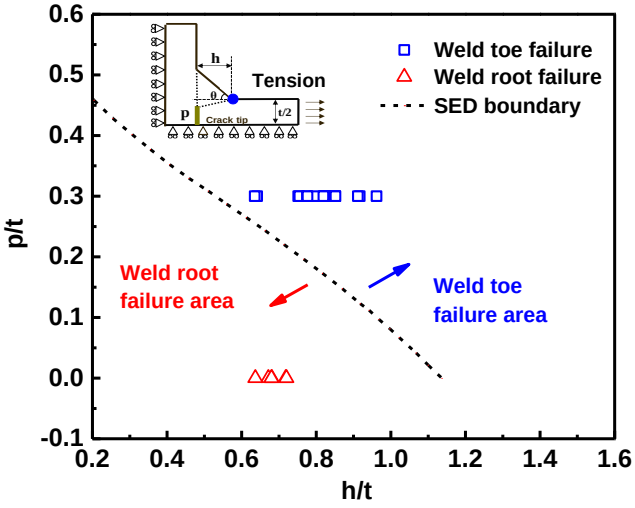

Fig. 14. Different fatigue failure locations according to SED boundary.

5 Conclusion

The paper presents new analytical equations for estimating SED values in LCWJ. The geometrical effects and loading conditions in LCWJ are systematically investigated using SED method. The corresponding analytical equations at weld toe and weld root under tension and bending loading are proposed. Thus, the failure modes of weld toe and weld root have been examined. The evolution of fatigue failure transition zone with the variation of flank angles is analyzed. Finally, the fatigue life assessment of the investigated 10CrNi3MoV high strength steel LCWJs is conducted and it further validates the feasibility of these analytical solutions based on SED, N-SIF and peak stress methods. The presented study leads to the

following findings:

(1) Comparison of NSIFs and SED values showed excellent agreement between numerical results and those predicted by proposed equations considering the pure tension and bending loadings.

(2) The critical weld size and failure transition were affected significantly by the flank angle at weld toe under tension loading in LCWJ. By increasing the angle from 30° to 60°, the boundary of weld toe and weld root failure was moved left in the range of 30° to 45°, then it moved right from 45° to 60°. Therefore, the transition boundary at 45° is the boundary limitation for weld toe and weld root.

(3) The analytical equations based on the SED approach were verified against 24 fatigue tests data of LCWJ. The comparison showed the enhanced correlation by the SED design scatter band considering different failure modes.

(4) The advantage of the proposed method is that it permits a fast evaluation of the SED, NSIFs and peak stress at weld toe and weld root in cruciform joints under tension or bending loading, without using complex and time-consuming FE calculations.

Reference

1. Radaj D (1996) Review of fatigue strength assessment of nonwelded and welded structures based on local parameters. *Int J Fatigue* **18**: 153-170.
2. Hobbacher AF (2016) Fatigue Design of Welded Joints and Components(Second Edition). *IIW document IIW-2259-15*.
3. Dong P (2001) A structural stress definition and numerical implementation for fatigue analysis of welded joints. *Int J Fatigue* **23**: 865-876.
4. Atzori B, Lazzarin P, Meneghetti G (2008) Fatigue strength assessment of welded joints: From the integration of Paris' law to a synthesis based on the notch stress intensity factors of the uncracked geometries. *Eng Fract Mech* **75**: 364-378.
5. Lazzarin P, Tovo R (1998) A notch intensity factor approach to the stress analysis of welds. *Fatigue Fract Eng Mater Struct* **21**: 1089-1103.
6. Lazzarin P, Berto F, Gomez FJ, Zappalorto M (2008) Some advantages derived from the use of the strain energy density over a control volume in fatigue strength assessments of welded joints. *Int J Fatigue* **30**: 1345-1357.
7. Lazzarin P, Berto F, Zappalorto M (2010) Rapid calculations of notch stress intensity factors based on averaged strain energy density from coarse meshes: Theoretical bases and applications. *Int J Fatigue* **32**: 1559-1567.
8. Berto F, Campagnolo A, Chebat F, Cincera M, Santini M (2016) Fatigue strength of steel rollers with failure occurring at the weld root based on the local strain energy values: modelling and fatigue assessment. *Int J Fatigue* **82**: 643-657.
9. Meneghetti G (2008) The peak stress method applied to fatigue assessments of steel and aluminium fillet-

welded joints subjected to mode I loading. *Fatigue Fract Eng Mater Struct* **31**: 346-369.

10. Meneghetti G, De Marchi A, Campagnolo A (2016) Assessment of root failures in tube-to-flange steel welded joints under torsional loading according to the Peak Stress Method. *Theor Appl Fract Mech* **83**: 19-30.
11. Meneghetti G, Campagnolo A, Avalle M, et al. (2018) Rapid evaluation of notch stress intensity factors using the peak stress method: Comparison of commercial finite element codes for a range of mesh patterns. *Fatigue Fract Eng Mater Struct* **41**: 1044-1063.
12. Nykänen T, Li X, Björk T, Marquis G (2005) A parametric fracture mechanics study of welded joints with toe cracks and lack of penetration. *Eng Fract Mech* **72**: 1580-1609.
13. Liu G, Liu Y, Huang Y (2014) A novel structural stress approach for multiaxial fatigue strength assessment of welded joints. *Int J Fatigue* **63**: 171-182.
14. Lazzarin P, Berto F, Atzori B (2013) A synthesis of data from steel spot welded joints of reduced thickness by means of local SED. *Theor Appl Fract Mech* **63-64**: 32-39.
15. Radaj D, Berto F, Lazzarin P (2009) Local fatigue strength parameters for welded joints based on strain energy density with inclusion of small-size notches. *Eng Fract Mech* **76**: 1109-1130.
16. Meneghetti G, Campagnolo A, Berto F (2015) Fatigue strength assessment of partial and full-penetration steel and aluminium butt-welded joints according to the peak stress method. *Fatigue Fract Eng Mater Struct* **38**: 1419-1431.
17. Meneghetti G, Campagnolo A, Rigon D (2017) Multiaxial fatigue strength assessment of welded joints using the Peak Stress Method – Part I: Approach and application to aluminium joints. *Int J Fatigue* **101**: 328-342.
18. Meneghetti G, Campagnolo A, Rigon D (2017) Multiaxial fatigue strength assessment of welded joints using the Peak Stress Method – Part II: Application to structural steel joints. *Int J Fatigue* **101**: 343-362.
19. Berto F, Lazzarin P, Yates JR (2011) Multiaxial fatigue of V-notched steel specimens: A non-conventional application of the local energy method. *Fatigue Fract Eng Mater Struct* **34**: 921-943.
20. Berto F, Campagnolo A, Lazzarin P (2015) Fatigue strength of severely notched specimens made of Ti-6Al-4V under multiaxial loading. *Fatigue Fract Eng Mater Struct* **38**: 503-517.
21. Pook LP, Campagnolo A, Berto F (2016) Coupled fracture modes of discs and plates under anti-plane loading and a disc under in-plane shear loading. *Fatigue Fract Eng Mater Struct* **39**: 924-938.
22. Campagnolo A, Meneghetti G, Berto F (2016) Rapid finite element evaluation of the averaged strain energy density of mixed-mode (I+II) crack tip fields including the T-stress contribution. *Fatigue Fract Eng Mater Struct* **39**: 982-998.
23. Gallo P, Sumigawa T, Kitamura T, Berto F (2016) Evaluation of the strain energy density control volume for a nanoscale singular stress field. *Fatigue Fract Eng Mater Struct* **39**: 1557-1564.
24. Gallo P, Berto F, Glinka G (2016) Generalized approach to estimation of strains and stresses at blunt V-notches under non-localized creep. *Fatigue Fract Eng Mater Struct* **39**: 292-306.
25. Berto F, Lazzarin P, Radaj D (2008) Fictitious notch rounding concept applied to sharp V-notches: Evaluation of the microstructural support factor for different failure hypotheses. Part I: Basic stress equations. *Eng Fract Mech* **75**: 3060-3072.
26. Berto F, Lazzarin P, Radaj D (2009) Fictitious notch rounding concept applied to sharp V-notches: Evaluation of the microstructural support factor for different failure hypotheses. Part II: Microstructural support analysis. *Eng Fract Mech* **76**: 1151-1175.
27. Pedersen MM (2016) Multiaxial fatigue assessment of welded joints using the notch stress approach. *Int J Fatigue* **83**: 269-279.

28. Pedersen MM, Mouritsen OO, Hansen MR, Andersen JG, Wenderby J (2010) Re-analysis of fatigue data for welded joints using the notch stress approach. *Int J Fatigue* **32**: 1620-1626.
29. Dong Y, Garbatov Y, Guedes Soares C (2018) Fatigue crack initiation assessment of welded joints accounting for residual stress. *Fatigue & Fracture of Engineering Materials & Structures*.
30. Möller B, Baumgartner J, Wagener R, Kaufmann H, Melz T (2017) Low cycle fatigue life assessment of welded high-strength structural steels based on nominal and local design concepts. *Int J Fatigue* **101**: 192-208.
31. Kainuma S, Mori T (2006) A fatigue strength evaluation method for load-carrying fillet welded cruciform joints. *Int J Fatigue* **28**: 864-872.
32. Zong L, Shi G, Wang Y-Q, Yan J-B, Ding Y (2017) Investigation on fatigue behaviour of load-carrying fillet welded joints based on mix-mode crack propagation analysis. *Archives of Civil and Mechanical Engineering*. **17**: 677-686.
33. Xing S, Dong P, Threstha A (2016) Analysis of fatigue failure mode transition in load-carrying fillet-welded connections. *Marine Structures*. **46**: 102-126.
34. Lazzarin P, Berto F, Zappalorto M, Meneghetti G (2009) Practical application of the N-sif approach in fatigue strength assessment of welded joints. *Welding in the World*. **53**: R76-R89.
35. Song W, Liu X, Berto F, Wang P, Fang H (2017) Fatigue failure transition analysis in load-carrying cruciform welded joints based on strain energy density approach. *Fatigue Fract Eng Mater Struct* **40**: 1164-1177.
36. Kainuma S, Kim I-T (2005) Fatigue strength evaluation of load-carrying cruciform fillet-welded joints made with mild steel plates of different thickness. *Int J Fatigue* **27**: 810-816.
37. Song W, Liu X, Berto F, Wang P, Xu J, Fang H (2017) Strain energy density based fatigue cracking assessment of load-carrying cruciform welded joints. *Theor Appl Fract Mech* **90**: 142-153.
38. Xing S, Dong P, Wang P (2017) A quantitative weld sizing criterion for fatigue design of load-carrying fillet-welded connections. *Int J Fatigue* **101**: 448-458.
39. Feng L, Qian X (2017) A hot-spot energy indicator for welded plate connections under cyclic axial loading and bending. *Eng Struct* **147**: 598-612.
40. Saiprasertkit K, Hanji T, Miki C (2012) Fatigue strength assessment of load-carrying cruciform joints with material mismatching in low- and high-cycle fatigue regions based on the effective notch concept. *Int J Fatigue* **40**: 120-128.
41. Saiprasertkit K, Hanji T, Miki C (2012) Local strain estimation method for low- and high-cycle fatigue strength evaluation. *Int J Fatigue* **40**: 1-6.
42. Branco R, Costa JDM, Berto F, et al. (2018) Low-cycle fatigue behaviour of AISI 18Ni300 maraging steel produced by selective laser melting. *Metals*. **8**.
43. Razavi SMJ, Bordonaro GG, Ferro P, Torgersen J, Berto F (2018) Fatigue behavior of porous Ti-6Al-4V made by laser-engineered net shaping. *Materials*. **11**.
44. Razavi SMJ, Ferro P, Berto F (2017) Fatigue assessment of Ti–6Al–4V circular notched specimens produced by selective laser melting. *Metals*. **7**.
45. Razavi SMJ, Ferro P, Berto F, Torgersen J (2017) Fatigue strength of blunt V-notched specimens produced by selective laser melting of Ti-6Al-4V. *Theor Appl Fract Mech.*
46. Livieri P, Lazzarin P (2005) Fatigue strength of steel and aluminium welded joints based on generalised stress intensity factors and local strain energy values. *Int J Fract* **133**: 247-276.
47. Gross B, Mendelson A (1972) Plane elastostatic analysis of V-notched plates. *Int J FractMech* **8**: 267-276.

48. Lazzarin P, Zambardi R (2001) A finite-volume-energy based approach to predict the static and fatigue behavior of components with sharp V-shaped notches. *Int J Fract* **112**: 275-298.
49. P. Bailey FB, E.R. Cawte, P. Roberts, M.T.. Whittaker, J.R. Yates (Eds.) (2017) Fatigue assessment of welded joints in large steel structures: a modified nominal stress definition. *7th International Conference on Durability and Fatigue*. 247-258.
50. Atzori B, Lazzarin P, Tovo R (1999) Stress field parameters to predict the fatigue strength of notched components. *J Strain Anal Eng Des* **34**: 437-453.
51. Dieter Radaj CMS, W. Fricke (2006) *Fatigue assessment of welded joints by local approaches*. Cambridge England.
52. Lazzarin P, Livieri P, Berto F, Zappalorto M (2008) Local strain energy density and fatigue strength of welded joints under uniaxial and multiaxial loading. *Eng Fract Mech* **75**: 1875-1889.
53. Meneghetti G, Lazzarin P (2011) The peak stress method for fatigue strength assessment of welded joints with weld toe or weld root failures. *Welding in the World*. **55**: 22-29.